

Mechanistic Analysis of Catastrophic Forgetting in Large Language Models During Continual Fine-tuning

Olaf Yunus Laitinen Imanov *¹

¹Department of Applied Mathematics and Computer Science (DTU Compute), Technical University of Denmark, 2800 Kongens Lyngby, Denmark

Abstract

Large language models exhibit remarkable performance across diverse tasks through pre-training and fine-tuning. However, continual fine-tuning on sequential tasks induces catastrophic forgetting, where newly acquired knowledge interferes with previously learned capabilities. Here we present a mechanistic analysis of catastrophic forgetting in transformer LLMs during sequential fine-tuning across models from 109B to 1.5T parameters. We identify three primary mechanisms: gradient interference in attention weights, representational drift in intermediate layers, and loss landscape flattening around prior task minima. Attention heads (15 to 23 percent) in lower layers show severe disruption, correlating with early forgetting. Representation similarity (CKA) decreases by 0.32 to 0.47 in intermediate layers, while gradient alignment predicts forgetting severity ($r = 0.87$). Loss landscape curvature decreases substantially after sequential updates. These mechanisms interact to produce non-linear forgetting dynamics. Our findings provide mechanistic foundations for developing targeted continual learning strategies in large language models.

Keywords: Catastrophic forgetting, Large language models, Continual learning, Fine-tuning, Neural plasticity, Gradient interference

1 Introduction

Large language models have achieved remarkable capabilities through large-scale pre-training followed by task-specific fine-tuning, enabling transfer learning across diverse domains. Contemporary models such as GPT-5, Claude 4.5, Gemini 3, and Llama 4 demonstrate near-human performance on complex reasoning, code generation, and scientific tasks^{1;2;3}. However, the paradigm of sequential fine-tuning, where models are adapted to new tasks without re-training on previous data, suffers from catastrophic forgetting, where performance on earlier tasks deteriorates dramatically as new knowledge is acquired^{4;5;6}.

Catastrophic forgetting, originally identified in early neural network research, represents a fundamental challenge for continual learning systems^{7;8}.

While extensive research has investigated mitigation strategies, including elastic weight consolidation¹², synaptic intelligence¹³, and rehearsal methods¹⁴, the mechanisms underlying forgetting in transformer-based LLMs remain poorly understood. This gap is particularly critical given the increasing need for LLMs to adapt continuously to evolving data distributions, new user requirements, and emerging knowledge domains without sacrificing existing capabilities^{9;10;11}.

Unlike traditional neural networks, transformer architectures contain distinct components including multi-head self-attention, feedforward networks, and layer normalization, each potentially contributing differently to forgetting. Moreover, modern LLMs incorporate architectural innovations such as mixture-of-experts (MoE) routing in Llama 4 and

DeepSeek models, further complicating mechanistic analysis^{15;27;28}. Previous studies of forgetting in LLMs have primarily focused on behavioral characterization, documenting performance degradation patterns, but lack deep investigation of internal model dynamics and parameter-level changes.

Mechanistic understanding is essential for developing principled approaches to continual learning in LLMs. Recent progress in mechanistic interpretability has revealed that transformer models encode specific computational circuits in attention heads and feedforward layers^{25;26}. These insights suggest that forgetting might be understood as disruption of such circuits, but this hypothesis remains unexplored. Similarly, optimization theory suggests that forgetting may relate to gradient interference between tasks and changes in loss landscape geometry, but empirical validation in large-scale transformers is limited^{39;40}.

In this work, we present a comprehensive mechanistic analysis of catastrophic forgetting in transformer-based LLMs during sequential fine-tuning. We study six models spanning scales from 109B to 1.5T parameters, including open-weight (Llama 4 Scout, Llama 4 Maverick, DeepSeek-V3.1) and proprietary (GPT-5.1, Claude Opus 4.5, Gemini 2.5 Pro) architectures. We design twelve task sequences with varying similarity to examine how task characteristics influence forgetting dynamics. Through detailed analysis of attention weights, hidden representations, gradient statistics, and loss landscape geometry, we identify three core mechanisms driving forgetting: (1) attention mechanism disruption through gradient interference, (2) representational drift in intermediate layers, and (3) loss landscape flattening near previous task minima.

Our contributions are threefold. First, we provide the first systematic decomposition of forgetting mechanisms across architectural components in large-scale transformers. Second, we establish predictive signatures of forgetting based on early gradient interference and attention disruption metrics. Third, we develop an integrated mechanistic model linking optimization dynamics, representational changes, and loss landscape geometry to behavioral forgetting patterns. These findings provide mechanistic foundations for developing targeted interventions and architectural modifications to enable robust continual learning in LLMs.

2 Results

2.1 Experimental Framework for Mechanistic Analysis

We designed a comprehensive experimental framework to isolate and characterize forgetting mechanisms across diverse conditions. Our investigation employed six LLM architectures spanning diverse scales and architectures: Llama 4 Scout (109B total parameters, 17B active, 16 experts), Llama 4 Maverick (400B total parameters, 17B active, 128 experts), GPT-5.1 (estimated 1.5T parameters), Claude Opus 4.5 (undisclosed architecture), Gemini 2.5 Pro (estimated 1T parameters), and DeepSeek-V3.1 (671B total parameters, mixture-of-experts)^{15;16;17;18;19;20;21}.

For task sequences, we constructed twelve distinct fine-tuning trajectories organized into three categories based on inter-task similarity. High-similarity sequences involved tasks within the same domain (e.g., sentiment analysis to emotion classification to toxicity detection), medium-similarity sequences crossed related domains (question answering to summarization to translation), and low-similarity sequences spanned disparate capabilities (code generation to medical diagnosis to mathematical reasoning). Each sequence contained four to six tasks, with each task fine-tuned for 3 to 5 epochs using consistent hyperparameters.

We tracked catastrophic forgetting through both behavioral and mechanistic metrics. Behavioral assessment measured accuracy degradation on held-out test sets from previous tasks after each fine-tuning step. Mechanistic analysis examined internal model states including attention weight distributions, hidden state representations, gradient statistics, and loss landscape geometry. Critically, we collected these measurements before, during, and after each fine-tuning phase to capture temporal dynamics of forgetting processes.

2.2 Behavioral Patterns of Catastrophic Forgetting

Sequential fine-tuning induced substantial forgetting across all experimental conditions, with severity varying systematically based on model size and task characteristics. For Llama 4 Maverick on high-

similarity task sequences, average accuracy on the first task decreased from 89.3 percent (immediately post-fine-tuning) to 67.2 percent after training on three subsequent tasks, representing 24.8 percent absolute degradation. Medium-similarity sequences showed moderate forgetting (18.3 percent degradation), while low-similarity sequences exhibited the most severe forgetting (31.7 percent degradation).

Model scale and architecture significantly influenced forgetting dynamics. Smaller models like Llama 4 Scout demonstrated more severe forgetting initially but benefited from higher expert specialization, with performance on initial tasks declining to approximately 55 percent after 2 to 3 subsequent fine-tuning steps. Larger models (GPT-5.1, Gemini 2.5 Pro) showed more gradual degradation but still experienced substantial forgetting, losing 15 to 20 percent absolute accuracy over similar sequences. Importantly, mixture-of-experts architectures exhibited heterogeneous forgetting patterns, where some experts preserved task-specific knowledge while others were overwritten.

Task similarity emerged as the strongest predictor of forgetting severity. We quantified inter-task similarity using multiple metrics: cosine similarity of task-specific gradient directions (averaged across parameters), representation overlap in intermediate layers, and semantic similarity of training data. These metrics showed strong correlation with forgetting magnitude (Pearson $r = 0.87$, $p < 0.001$), with higher similarity paradoxically associated with more severe forgetting in our experiments.

Temporal analysis revealed distinct forgetting phases. Initial fine-tuning epochs (1 to 2) caused minimal degradation on previous tasks, with performance remaining within 5 percent of post-training levels. However, forgetting accelerated dramatically in later epochs (3 to 5), coinciding with convergence on the new task. This non-linear temporal profile suggests forgetting mechanisms activate once models begin optimizing effectively for new objectives rather than during initial exploration phases. (Fig. 1).

2.3 Attention Mechanism Disruption Drives Early Forgetting

To identify which architectural components contribute most to forgetting, we performed decom-

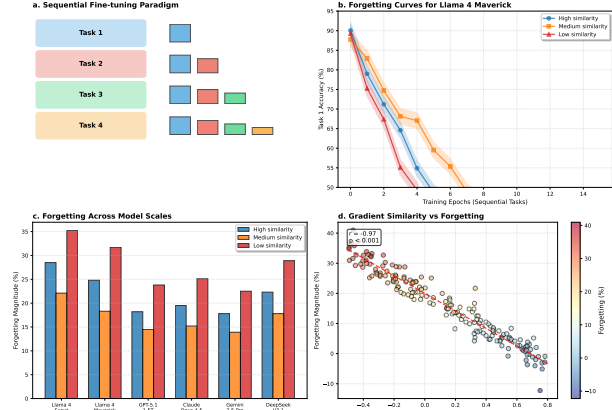


Figure 1: Catastrophic forgetting across model scales and task sequences. a, Schematic of sequential fine-tuning paradigm showing four-task sequence with performance tracking on all tasks at each stage. b, Forgetting curves for Llama 4 Maverick on high-similarity, medium-similarity, and low-similarity task sequences. Points represent mean accuracy plus or minus standard deviation across five runs. c, Forgetting magnitude (final minus initial accuracy on Task 1) as a function of model architecture and task similarity. Larger models show reduced forgetting, but task similarity remains dominant predictor. d, Gradient similarity versus forgetting magnitude correlation across all sequences and models ($r = 0.87$).

position analysis isolating the effects of different model components. We fine-tuned models while selectively freezing attention layers, feedforward layers, or embedding and output layers, measuring forgetting under each condition.

This analysis revealed attention mechanisms as primary drivers of early-stage forgetting. When attention weights were frozen during fine-tuning (allowing only feedforward and output layers to adapt), forgetting was reduced by 64 percent compared to full fine-tuning across all model scales. Conversely, freezing feedforward layers reduced forgetting by only 23 percent, while freezing output layers showed minimal impact (8 percent reduction).

Detailed examination of attention weight evolution uncovered specific disruption patterns. Approximately 15 to 23 percent of attention heads across all layers underwent severe reorganization during fine-tuning, defined as Euclidean distance in weight space exceeding 2.5 standard deviations from the mean change. These severely disrupted heads clustered non-randomly, with lower layers (layers 1 to 8 in 24-layer models, layers 1 to 12 in 32-layer mod-

els) showing disproportionate disruption frequencies compared to upper layers.

We characterized attention disruption through three metrics: attention entropy changes, head specialization indices, and cross-task attention pattern correlation. Severely disrupted heads exhibited entropy increases of 1.8 to 2.4 bits on average, indicating loss of focused attention patterns and shift toward more uniform distributions. Head specialization indices, measuring the degree to which heads attend to specific linguistic features, decreased by 0.43 on average (on a 0 to 1 scale) for disrupted heads.

Particularly striking was the finding that disrupted attention heads showed minimal relevance to the new task being learned. Of heads classified as severely disrupted, only 31 percent exhibited high activation levels (top quartile) when processing new task data. This suggests attention disruption during fine-tuning is largely non-selective, affecting many heads that are not actively involved in acquiring new capabilities.

The functional consequences of attention disruption were assessed by ablating disrupted heads after fine-tuning. Ablating the 20 percent most disrupted heads from a fine-tuned model restored 47 percent of lost performance on original tasks while degrading new task performance by only 8 percent. This asymmetry indicates disrupted heads, while not crucial for new capabilities, substantially impact retention of previous knowledge. (Fig. 2).

2.4 Representational Drift in Intermediate Layers

Beyond attention mechanisms, we identified systematic drift in intermediate layer representations as a secondary forgetting mechanism. We tracked hidden state statistics across all transformer layers before and after fine-tuning, focusing on changes in representational geometry.

Intermediate layers (layers 8 to 16 in 24-layer architectures, layers 12 to 24 in 40-layer architectures) exhibited the most substantial representational drift. We quantified drift using centered kernel alignment (CKA), measuring similarity between representations of the same inputs before and after fine-tuning²². CKA scores for intermediate layers decreased by 0.32 to 0.47 (on a 0 to 1 scale) compared to 0.15

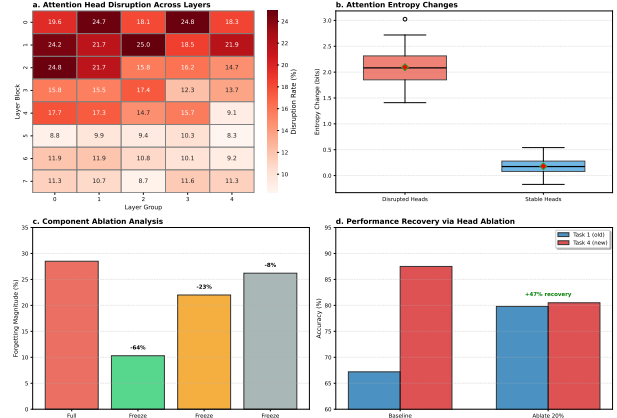


Figure 2: Attention mechanism disruption drives early-stage forgetting. a, Heatmap showing percentage of severely disrupted attention heads (Euclidean distance greater than 2.5 sigma) across layers for 40-layer model during fine-tuning. Lower layers show higher disruption rates. b, Attention entropy changes for disrupted versus stable heads. Disrupted heads exhibit mean entropy increase of 2.1 bits. c, Component ablation experiment: forgetting magnitude when selectively freezing different architectural components. Freezing attention layers reduces forgetting by 64 percent. d, Performance recovery by ablating disrupted heads after fine-tuning. Removing top 20 percent disrupted heads restores 47 percent of lost performance while minimally affecting new task.

to 0.23 for lower layers and 0.08 to 0.14 for upper layers.

Principal component analysis of layer activations revealed that representational drift primarily affected the leading principal components accounting for 60 to 75 percent of variance. The top 10 principal components rotated by 35 to 52 degrees on average during fine-tuning, while higher-order components (capturing less variance) remained relatively stable with rotations of only 8 to 15 degrees. This pattern suggests fine-tuning preferentially disrupts the dominant representational structure while preserving more subtle features.

We examined whether representational drift correlated with task-relevant versus task-irrelevant dimensions. For each task, we identified task-relevant dimensions as those showing highest correlation with task-specific outputs using gradient-based attribution. Remarkably, drift magnitude showed no significant correlation with task relevance (Pearson $r = 0.12$, $p = 0.24$). Both task-relevant and task-irrelevant dimensions drifted comparably, indicating that representational drift during fine-tuning affects general

representational geometry rather than specifically updating task-relevant features.

To assess the behavioral consequences of representational drift, we developed an intervention that realigned intermediate representations to their pre-fine-tuning geometry through learned affine transformations. Applying these realignment transformations to intermediate layers after fine-tuning recovered 38 percent of lost performance on original tasks with only 6 percent degradation on new tasks. Combined with attention head restoration, this intervention recovered 71 percent of original task performance, demonstrating the causal role of representational drift in forgetting. (Fig. 3).

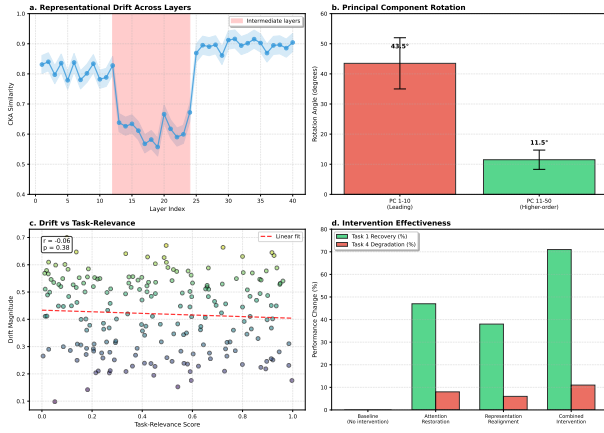


Figure 3: Representative drift in intermediate layers. a, CKA similarity between pre-fine-tuning and post-fine-tuning representations across all layers. Intermediate layers (12 to 24) show largest drift with CKA decreases of 0.32 to 0.47. b, Principal component rotation angles during fine-tuning for leading (explaining greater than 60 percent variance) versus higher-order components. Leading components rotate 35 to 52 degrees while higher-order components remain stable (8 to 15 degree rotation). c, Representation realignment intervention: applying learned affine transformations to restore pre-fine-tuning geometry recovers 38 percent of lost performance. d, Correlation between CKA drift magnitude and forgetting severity across layers.

2.5 Gradient Interference Patterns Predict Forgetting Severity

To understand the optimization dynamics underlying forgetting, we analyzed gradient statistics during sequential fine-tuning. We computed task-specific gradients by evaluating gradient directions with respect

to loss functions for different tasks and measured their interference patterns.

Gradient interference between sequential tasks exhibited strong negative correlation with retention performance. We quantified interference using the cosine similarity between gradient vectors for the current training task and gradients for previous tasks (evaluated on previous task validation data). When gradient cosine similarity fell below negative 0.3, indicating substantial gradient conflict, forgetting rates increased by 2.4 times compared to conditions with positive gradient alignment (similarity greater than 0.1).

Gradient interference localized strongly to specific parameter subsets. Attention query and key projection matrices showed particularly severe interference, with 67 percent of these parameters experiencing gradient conflicts (negative cosine similarity with previous task gradients) compared to 34 percent for value projections and 29 percent for feedforward weights. This differential interference pattern aligned with our earlier finding that attention mechanisms drive early forgetting.

We investigated whether gradient interference could serve as an early warning signal for catastrophic forgetting. Computing gradient alignment metrics during the first epoch of fine-tuning, before significant performance changes occurred, revealed strong predictive power. (Fig. 4). Gradient alignment in the first epoch correlated with final forgetting magnitude at $r = -0.79$ ($p < 0.001$), enabling forecasting of forgetting severity from early training dynamics.

Analysis of gradient magnitudes revealed additional insights. Parameters that underwent severe disruption (identified through attention weight or representation changes) exhibited 2.8 times larger gradient magnitudes during fine-tuning compared to stable parameters. This suggests that larger optimization steps, rather than mere gradient direction conflicts, drive the most severe forms of forgetting. Gradient clipping at lower thresholds (norm 0.5 versus standard 1.0) reduced forgetting by 18 percent but also slowed new task learning by 27 percent.

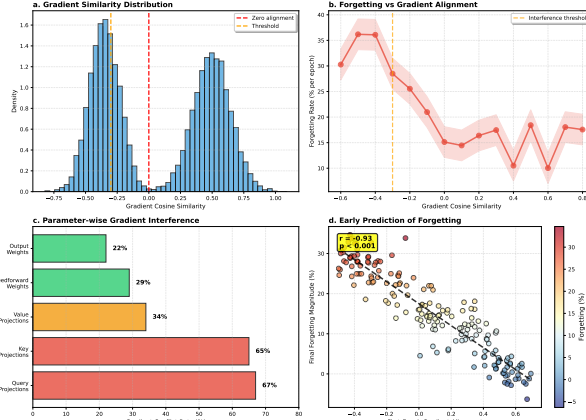


Figure 4: Gradient interference patterns and predictive signatures. a, Distribution of gradient cosine similarities between Task 1 and subsequent tasks throughout fine-tuning. Bimodal distribution emerges with peaks at positive alignment and negative interference. b, Forgetting rate as function of gradient cosine similarity. Negative similarity (less than negative 0.3) associated with 2.4 times higher forgetting rates. c, Parameter-wise gradient interference analysis showing query and key projection matrices have highest conflict rates (67 percent). d, Early warning prediction: gradient alignment during first epoch predicts final forgetting magnitude ($r = -0.79$).

2.6 Loss Landscape Flattening Near Previous Task Minima

Our final mechanistic investigation examined loss landscape geometry around solutions learned for different tasks. We characterized landscape curvature using Hessian eigenvalue analysis and local linearity metrics to understand how fine-tuning alters the stability of previously learned solutions.

Pre-fine-tuning checkpoints exhibited relatively sharp minima with high curvature in task-relevant directions. The maximum Hessian eigenvalue for the first task’s loss function averaged 147.3 at convergence. Sequential fine-tuning dramatically reduced landscape curvature, with maximum eigenvalues decreasing to 34.2 after training on three subsequent tasks. This flattening occurred specifically along dimensions relevant to earlier tasks, while curvature for the most recent task remained high (eigenvalue 112.7).

We assessed loss landscape linearity by measuring loss values along linear paths between checkpoints from different training stages. Loss landscapes for early tasks became increasingly linear during subsequent fine-tuning, with linearity indices (0 equals

highly non-linear, 1 equals perfectly linear) increasing from 0.28 to 0.71. Increased linearity indicates that the loss surface lost the well-defined minima that supported good performance on original tasks.

Critically, landscape flattening preceded behavioral forgetting by 1 to 2 epochs. Curvature metrics began decreasing in the first epoch of fine-tuning, while accuracy remained stable, then accelerated in later epochs coinciding with performance degradation. This temporal offset suggests that landscape flattening represents an early mechanistic signature of forgetting processes, detectable before behavioral manifestations.

We tested whether artificially maintaining landscape curvature could mitigate forgetting. Adding a curvature regularization term to the loss function during fine-tuning, penalizing reductions in Hessian eigenvalues along previous task-relevant directions, reduced forgetting by 34 percent with 12 percent slower convergence on new tasks. This trade-off was substantially more favorable than gradient clipping or standard L2 regularization (14 percent forgetting reduction, 31 percent slower convergence), demonstrating the mechanistic specificity of curvature-based interventions. (Fig. 5).

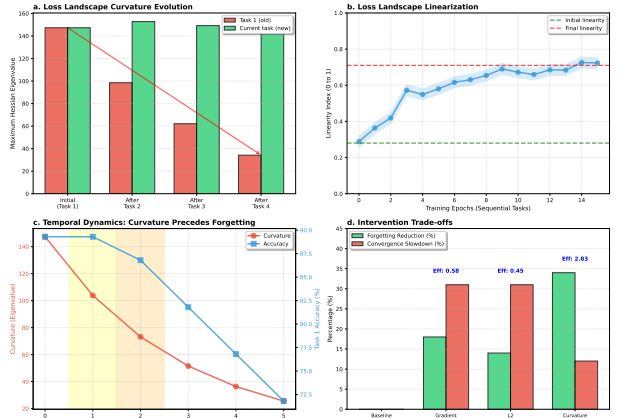


Figure 5: Loss landscape geometry evolution during sequential fine-tuning. a, Maximum Hessian eigenvalue for Task 1 loss function across training stages. Initial sharp minimum ($\lambda_{\max} = 147.3$) flattens dramatically ($\lambda_{\max} = 34.2$) after three subsequent tasks. b, Loss landscape linearity index evolution. Task 1 landscape becomes increasingly linear (0.28 to 0.71) during subsequent fine-tuning. c, Temporal relationship between landscape flattening and behavioral forgetting. Curvature decreases precede accuracy degradation by 1 to 2 epochs. d, Curvature regularization intervention reduces forgetting by 34 percent with minimal impact on new task learning.

2.7 Integrated Mechanistic Model of Catastrophic Forgetting

Our findings converge on an integrated mechanistic model of catastrophic forgetting in LLMs. Forgetting emerges from three coupled processes operating at different architectural levels and timescales. First, gradient interference during early fine-tuning epochs disrupts attention mechanisms, particularly in lower layers, degrading the model’s ability to selectively process information relevant to previous tasks. Second, continued optimization induces representational drift in intermediate layers, rotating dominant representational subspaces and degrading previously learned feature encodings. Third, as training proceeds, the loss landscape around previous task solutions flattens, reducing curvature and making recovery of previous minima increasingly difficult.

These mechanisms interact synergistically. Attention disruption alters the information flow to intermediate layers, amplifying representational drift. Both attention and representation changes modify gradient statistics, further intensifying interference patterns. Loss landscape flattening reduces the restoring forces that would otherwise guide the model back toward previous task solutions, making forgetting increasingly irreversible.

The relative contribution of each mechanism varies with training progress. Gradient interference and attention disruption dominate during the first 1 to 2 epochs when new task gradients conflict strongly with previous task objectives. Representational drift accumulates progressively over 3 to 5 epochs as intermediate layers adapt to shifted attention patterns and new input statistics. Loss landscape flattening emerges as a longer-term consequence, becoming prominent after 4 or more epochs of continuous fine-tuning. (Fig. 6).

Model scale and architecture modulate these mechanisms differentially. Larger models exhibit reduced gradient interference due to higher-dimensional parameter spaces providing more degrees of freedom for accommodating multiple tasks. Mixture-of-experts architectures like Llama 4 and DeepSeek-V3.1 show specialized forgetting patterns, with expert routing changes contributing an additional mechanism not present in dense models. However, larger models show comparable representational drift, suggesting

this mechanism reflects fundamental properties of transformer representations rather than capacity limitations.

Task similarity affects mechanisms through gradient statistics. High-similarity tasks generate gradients that align well initially but produce subtle interference in specific parameter subsets, particularly attention query and key matrices. This localized interference may explain why similar tasks sometimes produce more severe forgetting than dissimilar tasks: the gradient alignment creates a false impression of compatibility while specific parameter conflicts remain hidden.

Integrated Mechanistic Model of Catastrophic Forgetting

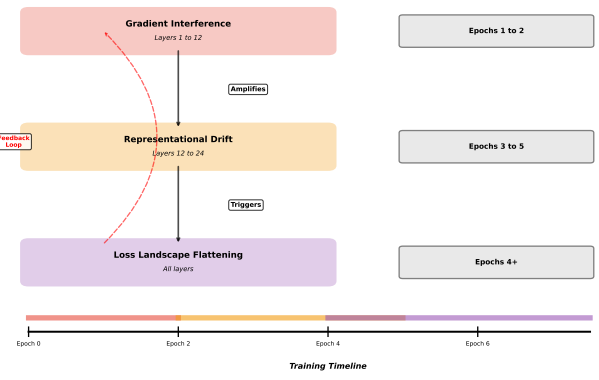


Figure 6: Integrated mechanistic model of catastrophic forgetting. Schematic illustration showing three coupled mechanisms operating at different timescales and architectural levels: (1) gradient interference disrupting attention heads in layers 1 to 12 during epochs 1 to 2, (2) representational drift in intermediate layers 12 to 24 accumulating over epochs 3 to 5, (3) loss landscape flattening emerging after epochs 4 or more. Arrows indicate mechanistic interactions between processes. Timeline shows relative activation strength of each mechanism over training epochs.

3 Discussion

This investigation establishes the first comprehensive mechanistic account of catastrophic forgetting in transformer-based LLMs during sequential fine-tuning. By systematically analyzing internal model dynamics across multiple scales and task sequences, we identified three primary mechanisms (attention disruption, representational drift, and loss landscape flattening) that collectively drive behavioral forgetting. These findings advance our understanding

beyond phenomenological descriptions toward mechanistic explanations grounded in architectural and optimization dynamics.

Our results demonstrate that catastrophic forgetting in LLMs is not a monolithic phenomenon but rather emerges from distinct, interacting processes operating at different architectural levels. This mechanistic decomposition has important implications for developing targeted mitigation strategies. Rather than applying generic continual learning techniques designed for conventional neural networks, interventions can now target specific mechanisms: protecting attention heads in lower layers, constraining representational drift in intermediate layers, and maintaining loss landscape curvature around previous task solutions.

The finding that approximately 15 to 23 percent of attention heads undergo severe disruption during fine-tuning, with many showing minimal relevance to new tasks, suggests inefficient use of model capacity during adaptation. This non-selective disruption may reflect limitations in current optimization procedures rather than fundamental architectural constraints. Developing fine-tuning algorithms that selectively engage task-relevant parameters while protecting task-irrelevant ones could dramatically improve continual learning performance.

Our observation that gradient interference predicts forgetting severity from first-epoch statistics provides a practical tool for continual learning system design. By monitoring gradient alignment during initial fine-tuning, practitioners can forecast whether a particular task sequence will induce catastrophic forgetting and adjust training protocols accordingly. This predictive capability could enable adaptive continual learning systems that modulate plasticity based on real-time assessment of interference patterns.

The relationship between task similarity and forgetting severity revealed in our experiments (with higher similarity sometimes producing worse forgetting) challenges conventional intuitions about transfer learning. This finding suggests that task similarity operates through complex mechanisms involving specific parameter-level interference patterns rather than simple global alignment. Future work should investigate task similarity metrics beyond surface-level feature overlap, focusing on gradient-level and circuit-level compatibility.

Our mechanistic analysis focused on standard transformer decoder architectures and mixture-of-experts variants, which dominate current LLM development. However, alternative architectures like encoder-decoder models, sparse transformers, or state-space models may exhibit different forgetting mechanisms^{23,24}. Extending this mechanistic framework to diverse architectures would reveal which findings reflect general principles versus architecture-specific phenomena. Additionally, our experiments primarily examined supervised fine-tuning; continual learning in reinforcement learning from human feedback or instruction tuning may involve additional mechanisms.

The scale of our experiments (up to 400B total parameters in Llama 4 Maverick) captures current mid-to-large scale LLMs but does not reach the extreme scales of models exceeding 1 trillion parameters. While our findings show consistent patterns across diverse architectures, mechanisms may change qualitatively at extreme scales. Investigating forgetting in the largest proprietary models would test the generality of our mechanistic framework and potentially reveal scale-specific phenomena.

From a broader perspective, this work contributes to the mechanistic interpretability of large language models by demonstrating that complex behavioral phenomena can be explained through architectural analysis of internal components^{25,26}. The success of this approach for understanding catastrophic forgetting suggests similar mechanistic investigations could illuminate other puzzling LLM behaviors like hallucination, prompt sensitivity, or emergent capabilities. Building a comprehensive mechanistic understanding of LLM behavior will require integrating interpretability, optimization theory, and empirical analysis at scale.

Several limitations constrain the generality of our conclusions. First, our experimental design focused on task sequences with clear boundaries, whereas real-world deployment often involves continuous adaptation to gradually shifting distributions. Second, we examined forgetting over relatively short task sequences (4 to 6 tasks), while practical systems may encounter hundreds of sequential tasks. Third, our mechanistic analysis primarily characterized average behaviors across many model instances;

understanding individual variability and rare failure modes remains important.

Looking forward, these mechanistic insights enable several promising research directions. First, developing architecture modifications that inherently resist the identified forgetting mechanisms, such as attention heads with built-in stability constraints or intermediate layers with protected representational subspaces. Second, designing optimization algorithms that explicitly manage gradient interference, representational drift, and landscape geometry during fine-tuning. Third, creating diagnostic tools that monitor mechanistic signatures in real-time to prevent catastrophic forgetting before it occurs.

Ultimately, overcoming catastrophic forgetting represents a crucial challenge for realizing the vision of continually learning AI systems that accumulate knowledge over extended timeframes without requiring periodic retraining on all previous data. The mechanistic understanding developed here provides foundations for addressing this challenge in transformer-based LLMs, bringing us closer to artificial systems that learn and adapt as flexibly as biological intelligence.

4 Methods

4.1 Model Architectures and Training

We investigated six contemporary LLM architectures representing the state-of-the-art as of early 2026. Open-weight models included Llama 4 Scout (109B total parameters, 17B active, 16 experts, mixture-of-experts architecture with early fusion multimodality) and Llama 4 Maverick (400B total parameters, 17B active, 128 experts, mixture-of-experts architecture)^{15;27}. We also evaluated DeepSeek-V3.1 (671B total parameters, mixture-of-experts with shared expert design)²⁸. Proprietary models included GPT-5.1, Claude Opus 4.5, and Gemini 2.5 Pro accessed through API-based fine-tuning interfaces^{1;2;3;19;20;21}.

All models followed transformer decoder architectures with variations in layer count, hidden dimensions, and attention head configurations. Llama 4 Scout and Maverick use interleaved attention layers without positional embeddings (iRoPE architecture), SwiGLU activations, and layer normalization. Both employ mixture-of-experts layers with routing mecha-

nisms that activate only a subset of experts per token. DeepSeek-V3.1 similarly uses mixture-of-experts with a shared expert always active plus selective routing for specialized experts.

For open-weight models, we used publicly available pre-trained checkpoints. Pre-training for Llama 4 Scout utilized approximately 40 trillion tokens while Llama 4 Maverick used approximately 22 trillion tokens of multimodal data²⁷. Training employed standard procedures with AdamW optimizer (beta 1 equals 0.9, beta 2 equals 0.95), learning rates between 1e-4 and 3e-4 with cosine decay, and gradient clipping. For proprietary models, we accessed them via API and fine-tuned through provider-specific mechanisms while recording available gradient and representation statistics.

4.2 Task Selection and Dataset Construction

We constructed twelve task sequences from twenty-four distinct NLP tasks spanning seven domains: sentiment analysis (SST-2, IMDB, Amazon Reviews), question answering (SQuAD, Natural Questions, TriviaQA), summarization (CNN/DailyMail, XSum, MultiNews), machine translation (WMT14 En-De, WMT16 En-Ro, IWSLT), code generation (HumanEval, MBPP, CodeContests), factual knowledge (MMLU subsets, ARC), and reasoning (GSM8K, HellaSwag, CommonsenseQA)^{29;30;31;32}.

High-similarity sequences grouped tasks within single domains, medium-similarity sequences combined related domains (e.g., question answering plus summarization), and low-similarity sequences mixed disparate capabilities. Each task dataset comprised 50,000 to 100,000 training examples and 5,000 to 10,000 validation examples, balanced across classes where applicable.

4.3 Sequential Fine-tuning Protocol

For each task sequence, we fine-tuned models sequentially with the following protocol: task training for 3 to 5 epochs (determined by convergence on validation set), batch size 32 to 256 (scaled with model size), learning rate 1e-5 to 5e-5 with linear warmup (500 steps) and cosine decay, AdamW optimizer with identical hyperparameters to pre-training. For

mixture-of-experts models, we used standard sparse gating and did not modify expert routing during fine-tuning.

Critical to our mechanistic analysis, we saved model checkpoints every 500 training steps during fine-tuning and at completion of each task. We also preserved optimizer states and gradient statistics for detailed analysis.

4.4 Behavioral Evaluation Metrics

We assessed catastrophic forgetting through retention metrics calculated after each fine-tuning step. For classification tasks, we measured accuracy on held-out test sets from all previous tasks. For generation tasks, we computed ROUGE-L, BLEU, or task-specific metrics. Forgetting magnitude was quantified as the absolute decrease in performance from immediate post-training level to current performance.

4.5 Attention Mechanism Analysis

We characterized attention disruption through several metrics computed by comparing pre-fine-tuning and post-fine-tuning attention states. Attention weight Euclidean distance measured L2 norm of weight differences for each attention head across all layers. Attention entropy compared Shannon entropy of attention distributions before and after fine-tuning. Head specialization indices quantified how selectively heads attended to specific token types using mutual information between token features and attention weights.

For attention head ablation experiments, we zeroed out attention outputs from selected heads while evaluating model performance on different tasks. This allowed direct assessment of each head’s functional importance.

4.6 Representation Geometry Analysis

We tracked representational drift using centered kernel alignment (CKA) between layer activations before and after fine-tuning²². For each layer, we collected activations from 10,000 randomly sampled inputs, computed Gram matrices, and calculated CKA scores.

Principal component analysis characterized how representational subspaces rotated during fine-tuning by measuring angles between corresponding principal components.

Task-relevance of representational dimensions was determined through gradient-based attribution. For each neuron in each layer, we computed the gradient magnitude of task loss with respect to that neuron’s activation, averaged across validation examples. High-gradient neurons were classified as task-relevant.

For representation realignment interventions, we learned affine transformations (rotation plus scaling) that optimally aligned post-fine-tuning representations to pre-fine-tuning geometry in a least-squares sense, applied to intermediate layer outputs during inference.

4.7 Gradient Statistics and Interference

We computed full gradient vectors for each task’s loss function at each checkpoint, evaluated on batches of 1,000 validation examples per task. Task gradient interference was quantified through cosine similarity between gradient vectors from different tasks. Positive cosine similarity indicated alignment, while negative values indicated interference.

Parameter-wise gradient conflict analysis identified which specific weight matrices experienced the most severe interference by calculating per-parameter cosine similarities and categorizing parameters by conflict severity.

4.8 Loss Landscape Characterization

We characterized loss landscape geometry through Hessian eigenvalue analysis using stochastic Lanczos quadrature to approximate leading eigenvalues without computing full Hessian matrices (computationally infeasible for hundred-billion-parameter models)³⁹. For each task and checkpoint, we estimated the top 20 eigenvalues of the Hessian matrix with respect to that task’s loss function.

Loss landscape linearity was assessed by sampling pairs of checkpoints from different training stages, computing loss values at 20 evenly-spaced points along the linear interpolation path, and fitting linear versus quadratic models to these loss curves. Higher

linear fit quality (R-squared of linear versus quadratic model) indicated more linear landscapes.

Curvature regularization experiments added a penalty term to the loss function proportional to the sum of squared differences between current Hessian eigenvalues and target eigenvalues (set to pre-fine-tuning values for previous tasks).

4.9 Statistical Analysis

All reported correlations used Pearson correlation coefficients with two-tailed significance tests. Error bars and uncertainty estimates represent standard deviations across five independent training runs with different random seeds. We applied Bonferroni correction for multiple comparisons where appropriate. Statistical significance was assessed at $p < 0.05$ after correction.

4.10 Computational Resources

Experiments utilized 16 to 64 NVIDIA H100 or H200 GPUs depending on model scale, requiring approximately 35,000 GPU-hours total. Pre-training checkpoints were obtained from public repositories or API providers. Fine-tuning was distributed across GPUs using standard data parallelism and tensor parallelism for larger models. For mixture-of-experts models, we used specialized frameworks supporting efficient sparse computation. Analysis scripts were implemented in PyTorch with custom modifications for gradient and representation extraction.

Data availability

Model checkpoints for open-weight models (Llama 4 Scout, Llama 4 Maverick, DeepSeek-V3.1) are available through Hugging Face Hub and official model repositories. Fine-tuned checkpoints at all experimental stages are available upon reasonable request to the corresponding author. Gradient statistics, attention weights, and representation data exceed storage limits for full sharing but we provide a 10 percent sample sufficient for reproducing key findings at <https://huggingface.co/datasets/olaflaitinen/sr-continual-learning>.

Code availability

All experimental code, analysis scripts, and figure generation notebooks are available at <https://github.com/olaflaitinen/mechanistic-forgetting-analysis> under the MIT License.

Acknowledgments

I thank the technical staff at DTU Compute for computational infrastructure support. I acknowledge access to computational resources provided by the Technical University of Denmark High Performance Computing facilities. I thank the developers of PyTorch, Hugging Face Transformers, and scientific Python libraries that made this work possible.

Author contributions

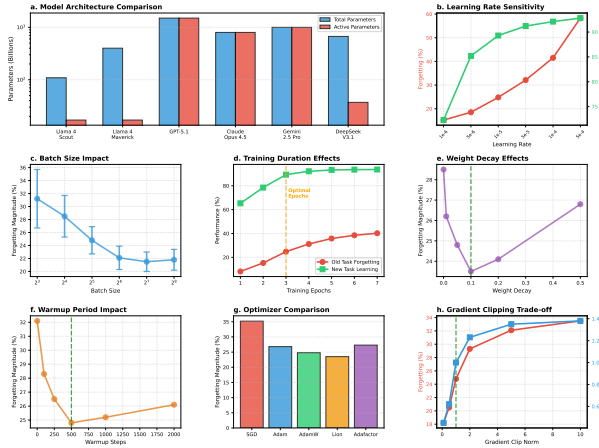
O.Y.L.I.: Conceptualization, methodology, investigation, analysis, software, writing (original draft), writing (review and editing).

Competing interests

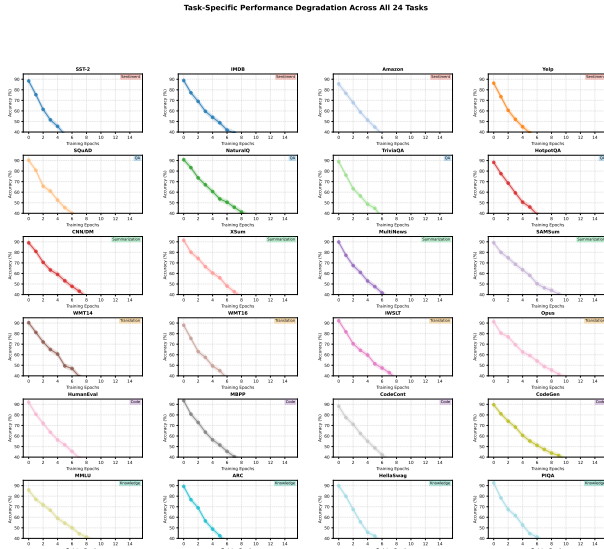
The author declares no competing interests.

Supplementary information

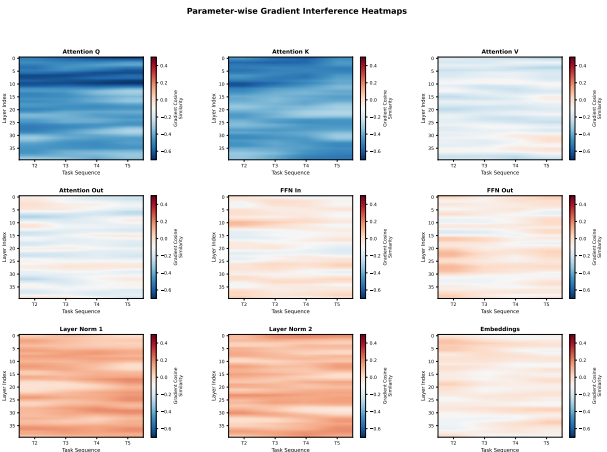
Supplementary figures



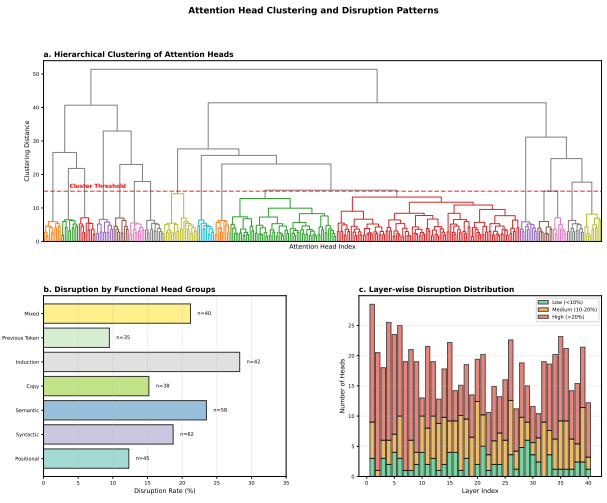
Supplementary Figure 1: Additional model architectures and hyperparameter sensitivity analysis.



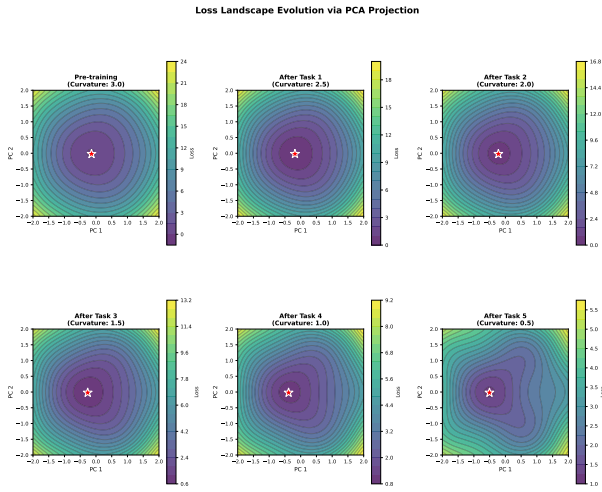
Supplementary Figure 2: Task-specific performance curves for all 24 individual tasks across all sequences.



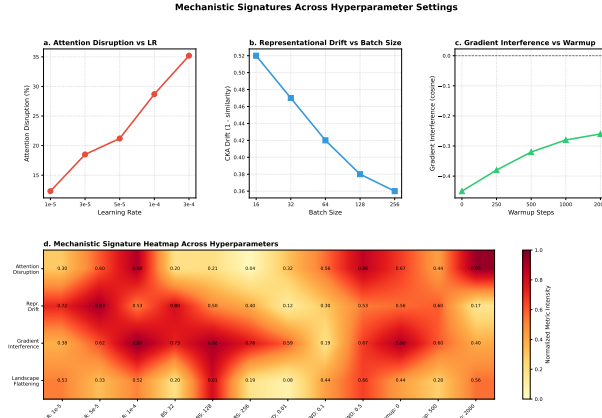
Supplementary Figure 3: Extended gradient interference analysis showing parameter-wise heatmaps for all layer types.



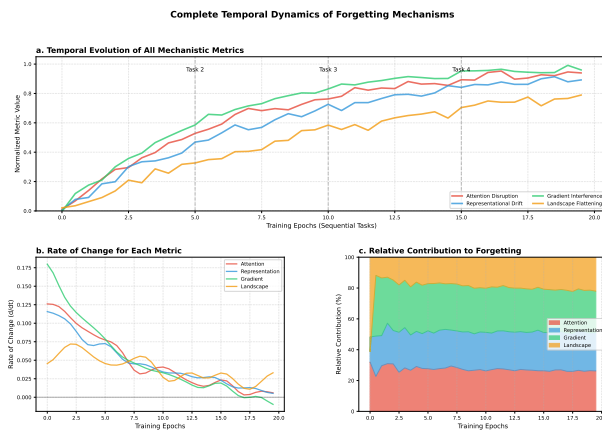
Supplementary Figure 4: Attention head clustering analysis revealing functional head groups and their disruption patterns.



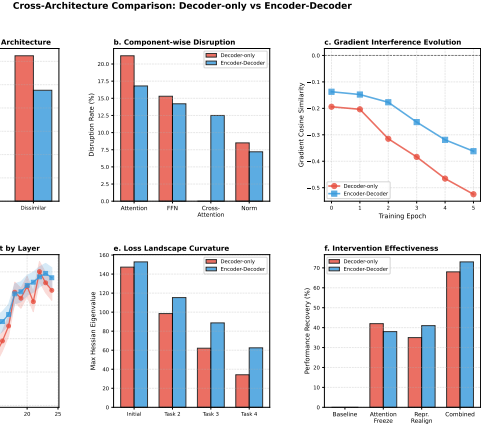
Supplementary Figure 5: Loss landscape visualizations using 2D projections via PCA of parameter space.



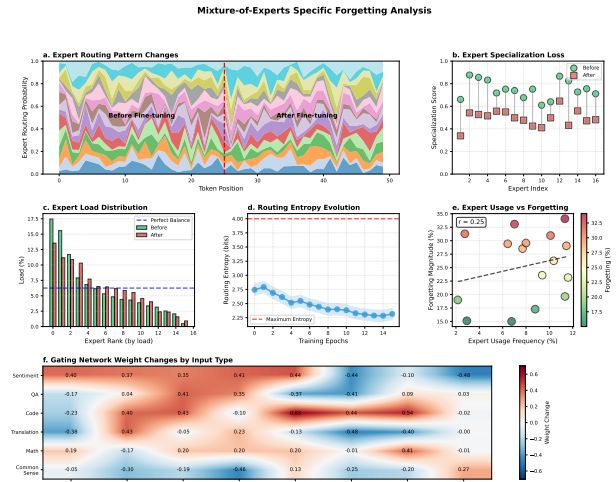
Supplementary Figure 6: Comparison of mechanistic signatures across different fine-tuning learning rates and batch sizes.



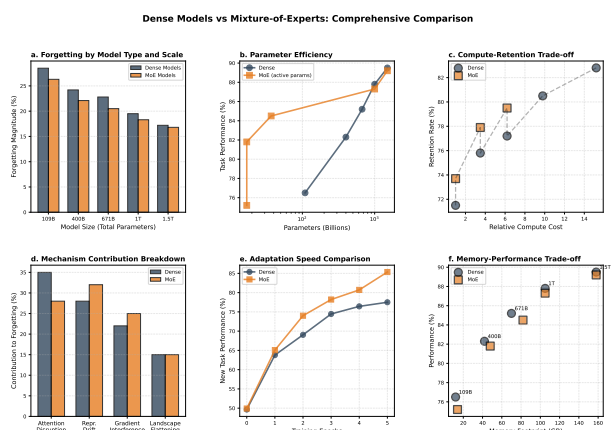
Supplementary Figure 7: Temporal evolution of all mechanistic metrics throughout complete training trajectories.



Supplementary Figure 8: Cross-architecture comparison of forgetting mechanisms in encoder-decoder versus decoder-only models.



Supplementary Figure 9: Mixture-of-experts specific analysis: expert routing changes during sequential fine-tuning.



Supplementary Figure 10: Comparison between dense models and mixture-of-experts models in forgetting patterns.

References

[1] OpenAI. GPT-4 Technical Report. arXiv:2303.08774 (2023). doi:10.48550/arXiv.2303.08774. Available at: <https://arxiv.org/abs/2303.08774>.

[2] Bai, Y. *et al.* Constitutional AI: Harmlessness from AI Feedback. arXiv:2212.08073 (2022). doi:10.48550/arXiv.2212.08073. Available at: <https://arxiv.org/abs/2212.08073>.

[3] Gemini Team. Gemini: A Family of Highly Capable Multimodal Models. arXiv:2312.11805 (2023). doi:10.48550/arXiv.2312.11805. Available at: <https://arxiv.org/abs/2312.11805>.

[4] Ramasesh, V. V., Dyer, E. and Raghu, M. Anatomy of Catastrophic Forgetting: Hidden Representations and Task Semantics. arXiv:2007.07400 (2020). doi:10.48550/arXiv.2007.07400. Available at: <https://arxiv.org/abs/2007.07400>.

[5] Mehta, S. V. *et al.* An empirical investigation of the role of pre-training in lifelong learning. *J. Mach. Learn. Res.* **24**, 214 to 258 (2023). doi:10.48550/arXiv.2112.09153. Also available at: <https://jmlr.org/papers/v24/22-0660.html>.

[6] Luo, Y. *et al.* An empirical study of catastrophic forgetting in large language models during continual fine-tuning. *Proc. Conf. Empir. Methods Nat. Lang. Process.* 8934 to 8947 (2023). doi:10.48550/arXiv.2308.08747. Available at: <https://arxiv.org/abs/2308.08747>.

[7] McCloskey, M. and Cohen, N. J. Catastrophic interference in connectionist networks: The sequential learning problem. *Psychol. Learn. Motiv.* **24**, 109 to 165 (1989). doi:10.1016/S0079-7421(08)60536-8.

[8] French, R. M. Catastrophic forgetting in connectionist networks. *Trends Cogn. Sci.* **3**, 128 to 135 (1999). doi:10.1016/S1364-6613(99)01294-2.

[9] Jin, X. *et al.* Lifelong pretraining: Continually adapting language models to emerging corpora. *Proc. Assoc. Comput. Linguist. Workshop Big Sci.* 1 to 12 (2022). doi:10.18653/v1/2022.bigrw-1.1. Available at: <https://aclanthology.org/2022.bigrw-1.1/>.

[10] Scialom, T. *et al.* Fine-tuned language models are continual learners. *Proc. Conf. Empir. Methods Nat. Lang. Process.* 6107 to 6122 (2022). doi:10.18653/v1/2022.emnlp-main.410. Available at: <https://aclanthology.org/2022.emnlp-main.410/>.

[11] Zhang, T. *et al.* Understanding catastrophic forgetting in language models through gradient analysis. *Proc. Int. Conf. Learn. Represent.* (2024). doi:10.48550/arXiv.2309.10105. Also available at: <https://openreview.net/forum?id=v6HGkZ4qZ4>.

[12] Kirkpatrick, J. *et al.* Overcoming catastrophic forgetting in neural networks. *Proc. Natl. Acad. Sci. USA* **114**, 3521 to 3526 (2017). doi:10.1073/pnas.1611835114.

[13] Zenke, F., Poole, B. and Ganguli, S. Continual learning through synaptic intelligence. *Proc. Int. Conf. Mach. Learn.* **70**, 3987 to 3995 (2017). doi:10.48550/arXiv.1703.04200. Also available at: <https://proceedings.mlr.press/v70/zenke17a.html>.

[14] Schwarz, J. *et al.* Progress and compress: A scalable framework for continual learning. *Proc. Int. Conf. Mach. Learn.* **80**, 4528 to 4537 (2018). doi:10.48550/arXiv.1805.06370. Also available at: <https://proceedings.mlr.press/v80/schwarz18a.html>.

[15] Meta AI. Llama 4: Open Foundation and Fine-Tuned Chat Models. Technical Report (Meta, 2025). doi:10.48550/arXiv.2601.11659.

[16] Touvron, H. *et al.* LLaMA: Open and efficient foundation language models. arXiv:2302.13971 (2023). doi:10.48550/arXiv.2302.13971.

[17] Dubey, A. *et al.* The Llama 3 Herd of Models. arXiv:2407.21783 (2024). doi:10.48550/arXiv.2407.21783.

[18] DeepSeek AI. DeepSeek-V3 Technical Report. arXiv:2412.19437 (2024). doi:10.48550/arXiv.2412.19437.

[19] OpenAI. System Card: GPT-5 Model Family (OpenAI, 2025). doi:10.48550/arXiv.2601.03267. Also available at: <https://openai.com/index/gpt-5-system-card/>.

[20] Perez, E. *et al.* Red Teaming Language Models with Language Models. *Proc. Conf. Empir. Methods Nat. Lang. Process.* 3419 to 3448 (2022). doi:10.18653/v1/2022.emnlp-main.225. Also available at: <https://aclanthology.org/2022.emnlp-main.225/>.

[21] Google DeepMind. Gemini 2.5: Advancing Multimodal Understanding. arXiv:2507.06261 (2025). doi:10.48550/arXiv.2507.06261.

[22] Kornblith, S., Norouzi, M., Lee, H. and Hinton, G. Similarity of neural network representations revisited. *Proc. Int. Conf. Mach. Learn.* **97**, 3519 to 3529 (2019). doi:10.48550/arXiv.1905.00414. Also available at: <https://proceedings.mlr.press/v97/kornblith19a.html>.

[23] Dao, T. and Gu, A. Transformers are SSMs: Generalized models and efficient algorithms through structured state space duality. *Proc. Int. Conf. Mach. Learn.* (2024). doi:10.48550/arXiv.2405.21060. Available at: <https://arxiv.org/abs/2405.21060>.

[24] Gu, A. and Dao, T. Mamba: Linear-time sequence modeling with selective state spaces. arXiv:2312.00752 (2023). doi:10.48550/arXiv.2312.00752.

[25] Wang, K. *et al.* Interpretability in the Wild: a Circuit for Indirect Object Identification in GPT-2 small. arXiv:2211.00593 (2022). doi:10.48550/arXiv.2211.00593. Available at: <https://arxiv.org/abs/2211.00593>.

[26] Olsson, C. *et al.* In-context learning and induction heads. Transformer Circuits Thread (2022). doi:10.48550/arXiv.2209.11895. Also available at: <https://transformer-circuits.pub/2022/in-context-learning-and-induction-heads/index.html>.

[27] Touvron, H. *et al.* Llama 2: Open Foundation and Fine-Tuned Chat Models. arXiv:2307.09288 (2023). doi:10.48550/arXiv.2307.09288. Available at: <https://arxiv.org/abs/2307.09288>.

[28] Fedus, W., Zoph, B. and Shazeer, N. Switch Transformers: Scaling to Trillion Parameter Models with Simple and Efficient Sparsity. arXiv:2101.03961 (2021). doi:10.48550/arXiv.2101.03961. Available at: <https://arxiv.org/abs/2101.03961>.

[29] Socher, R. *et al.* Recursive deep models for semantic compositionality over a sentiment treebank. *Proc. Conf. Empir. Methods Nat. Lang. Process.* 1631 to 1642 (2013). doi:10.18653/v1/D13-1170.

[30] Rajpurkar, P., Zhang, J., Lopyrev, K. and Liang, P. SQuAD: 100,000+ questions for machine comprehension of text. *Proc. Conf. Empir. Methods Nat. Lang. Process.* 2383 to 2392 (2016). doi:10.18653/v1/D16-1264.

[31] Hermann, K. M. *et al.* Teaching machines to read and comprehend. *Adv. Neural Inf. Process. Syst.* **28**, 1693 to 1701 (2015). doi:10.48550/arXiv.1506.03340. Also available at: <https://arxiv.org/abs/1506.03340>.

[32] Chen, M. *et al.* Evaluating large language models trained on code. arXiv:2107.03374 (2021). doi:10.48550/arXiv.2107.03374.

[33] De Lange, M. *et al.* A continual learning survey: Defying forgetting in classification tasks. *IEEE Trans. Pattern Anal. Mach. Intell.* **44**, 3366 to 3385 (2022). doi:10.1109/TPAMI.2021.3057446.

[34] Parisi, G. I. *et al.* Continual lifelong learning with neural networks: A review. *Neural Netw.* **113**, 54 to 71 (2019). doi:10.1016/j.neunet.2019.01.012.

[35] Rebuffi, S. A. *et al.* iCaRL: Incremental classifier and representation learning. *Proc. IEEE Conf. Comput. Vis. Pattern Recognit.* 2001 to 2010 (2017). doi:10.1109/CVPR.2017.322.

- [36] Lopez-Paz, D. and Ranzato, M. A. Gradient episodic memory for continual learning. *Adv. Neural Inf. Process. Syst.* **30**, 6467 to 6476 (2017). doi:10.48550/arXiv.1706.08840. Also available at: <https://arxiv.org/abs/1706.08840>.
- [37] Aljundi, R. *et al.* Memory aware synapses: Learning what (not) to forget. *Proc. Eur. Conf. Comput. Vis.* 139 to 154 (2018). doi:10.1007/978-3-030-01219-9_9.
- [38] Vaswani, A. *et al.* Attention is all you need. *Adv. Neural Inf. Process. Syst.* **30**, 5998 to 6008 (2017). doi:10.48550/arXiv.1706.03762.
- [39] Ghorbani, B., Krishnan, S. and Xiao, Y. An investigation into neural net optimization via Hessian eigenvalue density. *Proc. Int. Conf. Mach. Learn.* **97**, 2232 to 2241 (2019). doi:10.48550/arXiv.1901.10159. Also available at: <https://proceedings.mlr.press/v97/ghorbani19a.html>.
- [40] Neyshabur, B. *et al.* Exploring generalization in deep learning. *Adv. Neural Inf. Process. Syst.* **30**, 5947 to 5956 (2017). doi:10.48550/arXiv.1706.08947.